An Engineering Approach to Computational Prediction of Breakdown in Air With Surface Charging Effects

Pedersen, P.A. & Balszczyk, A.

Citation for the published version (APA 6th)
Pedersen, P. A., & Blaszczyk, A. (2017). An Engineering Approach to Computational Prediction of Breakdown in Air With Surface Charging Effects. *IEEE transactions on dielectrics and electrical insulation, 24*(5), 2775-2783. doi: http://dx.doi.org10.1109/TDEI.2017.006650

An Engineering Approach to Computational Prediction of Breakdown in Air with Surface Charging Effects

Atle Pedersen
SINTEF Energy Research
Department of Electric Power Technology
7465 Trondheim, Norway

and **Andreas Blaszczyk**
ABB Corporate Research
Department of Power Devices and Sensors
5405 Baden-Dättwil, Switzerland

ABSTRACT

This paper presents a dielectric simulation approach for predicting withstand voltage of air insulated power devices. The paper gives an overview of typical evaluation procedures for the basic discharge stages including inception, streamer propagation and leader transition. For selected test arrangements, we compare the results of lightning impulse tests with simulations. The simulations utilize a new approach that combines the well-established empirical procedure with numerical computations for arbitrary geometries. We introduce a new formulation for evaluation of saturation charge density, which enables a revision of the streamer inception conditions due to surface charging and an estimation of the leader transition characteristics including the surface capacitance.

Index Terms — **Dielectric breakdown, flashover, surface charging, dielectric measurement, simulation.**

1 INTRODUCTION

The goal of dielectric designing of high voltage equipment is to predict the necessary withstand voltage U_w in order to pass the required tests. It involves quantitative assessment of the discharge process including inception and propagation of streamers, which are the basic precursors for dielectric breakdown in inhomogeneous electric fields. Designers of high and medium voltage equipment typically utilize semi-empirical behavioural rules characterizing the discharge, described in engineering handbooks [1 - 3]. Recently, researchers have invested a significant effort to develop first principle simulations (e.g. [4]); however, such complex approaches are rarely usable for simulation procedures in industrial design of real devices. Therefore, the focus in this study is on an engineering approach that combines the empirical observations with numerical computations.

In this paper, we extend the discharge evaluation models and their applications presented in [5] and [6]. Section 2 contains an overview of streamer inception, propagation and leader transition rules in atmospheric air that are valid for the medium voltage range (test voltage levels below 100 kV/peak for AC, and up to 200 kV for standard lightning impulse 1.2/50 μs). In Sections 3 - 4 we present our experimental setup and results as well as a new simulation approach based on evaluation of surface charging. The new approach together with the traditional discharge model enables improved prediction of the withstand voltage, which is then discussed in Section 5.

2 OVERVIEW OF DISCHARGE PREDICTION PROCEDURES

2.1 CLASSIFICATION OF DISCHARGE PHENOMENA

The basic discharge phenomena relevant for prediction of the dielectric withstand are inception, streamer propagation and transition to leader. We illustrate all these discharge stages for an example case of a spherical high voltage (HV) electrode and a grounded plane (see Figure 1 and Table 1).

2.2 INCEPTION

After the appearance of an initial electron in a critical high field volume, an electron avalanche starts to develop. If a critical number N_c of electrons are generated, a self-propagating streamer head forms. The inception criterion is

$$\int_{\gamma} \alpha_{eff}(E)dx >= \ln(N_C) \tag{1}$$

where $\alpha_{eff}(E)$ is the field dependent effective ionization coefficient accounting for ionization, electron attachment, and detachment. The integration must be performed along a path γ where $\alpha_{eff} > 0$, starting from the point with maximum field strength and ending where $\alpha_{eff} = 0$ (at the critical field for which the ionization starts: 2.6 kV/mm for atmospheric air). We define E as the field strength component that is tangential to the path

Manuscript received on 17 February 2017, in final form 23 June 2017, accepted 24 June 2017. Corresponding author: A. Pedersen.

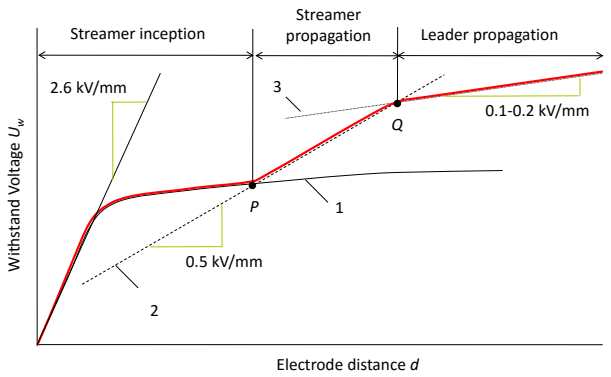

Figure 1. Sketch of withstand voltage U_w (thick red curve) determined by 3 different stages of discharge development. The explanation of all stages has been presented for a sphere-plane arrangement in Table 1.

γ. It follows, then, that for a path along a field line, E is equal to the absolute field. However, for a path along a dielectric surface, the tangential component is smaller in magnitude than the absolute. We use the empirically estimated values of $\alpha_{eff}(E)$ and $\ln(N_c) \approx$ 9-10 from [7] , which have been proven over many years of application. We calculate the value of inception voltage U_i iteratively by changing the applied voltage and scaling the E-field values until the inception equation (1) is satisfied.

For illustration, the curve 1 in Figure 1 shows qualitatively the relationship between U_i and the electrode separation distance d. The point P denotes the border between weakly and strongly inhomogeneous fields. The two first columns in Table 1 represent the geometry where the withstand voltage can be estimated directly from the inception voltage.

For smaller distances d up to the point P, the streamer inception is immediately followed by breakdown. The withstand voltage U_w is determined by U_i. Thus, U_w can be calculated using equation (1) and numerical field simulations. Due to surface roughness it may be necessary to reduce the withstand voltage below the inception level according to empirical roughness factor. However, atmospheric air has shown to be mostly insensitive to rough surfaces and reduction is limited to ~4 % for roughness up to 100 μm [1, 2].

2.3 STREAMER PROPAGATION

Streamer propagation needs to be considered when the field becomes strongly inhomogeneous. After streamer inception, a streamer head will propagate towards the opposite electrode. It will reach this electrode only if the applied voltage is large enough to maintain the propagation process. Locally, this means that the field in front of the streamer head must satisfy a criterion analogous to the inception criterion; this requires a sufficiently high voltage drop between streamer head and counter electrode. The lowest voltage (in kV) that enables a breakdown in an inhomogeneous field, can be approximately expressed (valid for distances larger than 40-50 mm) as follows [1 - 3]:

$$U_{ws} = U_0 + d \cdot E_{st} \qquad (2)$$

where d is the distance between electrodes in mm. E_{st} is the internal field strength in kV/mm along the (positive) streamer behind its head, and has the same value as the required external field for stable streamer propagation (**stability field**). The voltage $U_0 \approx$ 20-30 kV is equivalent to the potential of the streamer head needed to generate a breakdown.

The value of E_{st} may vary in the range of +/-10-20%, depending on various conditions like humidity (dry air: 0.4 kV/mm), voltage shape (AC: 0.45 kV/mm; impulse: 0.54 kV/mm) etc. The negative streamers require considerably higher internal field strength for stable propagation (up to 1.2 kV/mm). For evaluations in this paper, we assume for positive impulse: E_{st} = 0.54 kV/mm and U_0 = 23.4 kV.

The dashed curve 2 in Figure 1 corresponds to the stability field rule (2), and Table 1 shows the typical application cases in columns 3 and 4. Interestingly, the stability field rule is applicable for not only the straight gaps between electrodes, but also for arrangements where streamers propagate parallel to dielectric surfaces [8 - 10] or have to bypass barriers. The experimental results confirm that the withstand voltage is well

Table 1. Illustration of discharge stages for the arrangement sphere-plane.

Inception		Streamer Propagation		Leader propagation	
Homogenous	In-homogenous	Strongly inhomogenoues	Barriers	Strongly inhomogenoues – large distance	Embedded/coated electrodes
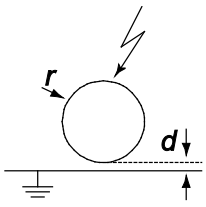	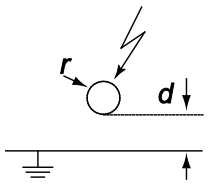	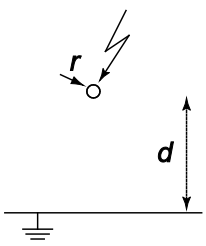	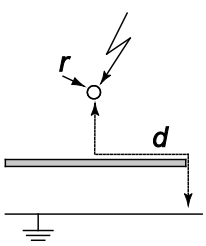	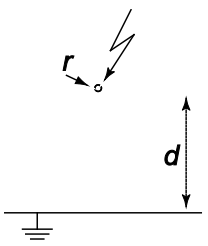	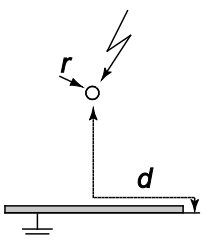
$d << r$	r is in same range as d	$d >> r$ $d <$ 2m	Discharge is bypassing a dielectric barrier.	$d >> r$ $d >$ 2m	Discharge is gliding along dielectric coating.

correlated with barrier overhang, which extends the discharge length *d* [11].

2.4 LEADER TRANSITION

Leader transition must be taken into account for longer air gaps over 2 m as indicated in the fifth column in Table 1. However, the transition to a leader for medium voltage is typically restricted to discharges propagating along dielectric surfaces, in particular along electrodes coated with an insulating layer as shown in last column in Table 1. Due to thermo-ionization effects the internal field strength E_L needed for leader propagation is below 0.1 - 0.2 kV/mm. Hence, the leader can propagate over longer distances than a streamer. In Figure 1 the dotted curve 3 represents the withstand voltage determined by leader propagation. It illustrates the significant reduction of U_w beyond the leader transition point *Q*.

The leader transition depends on its capacitive coupling with the surrounding electrodes. One can obtain the voltage required for leader transition of a discharge propagating along an insulating layer from the following empirical rule [2,3]:

$$U_{0L} = 0.000192 \cdot (10^{-10} \cdot c')^{-0.44} \quad (3)$$

where *c'* is the surface capacitance of the insulating layer in pF/mm^2 (*c'* >= 0.0025 pF/mm^2) and U_{0L} is in kV.

In order to avoid leader transition and the risk of punctures, the withstand voltage for arrangements with insulation layers can be conservatively evaluated using equation (3). However, U_{0L} specifies only the limit for the voltage across the insulation layer. The corresponding limit for the applied voltage is obtained from numerical field computation (see section 4.4) or roughly approximated, by adding U_{0L} to the voltage drop along the streamer reaching the insulation layer (see last column of Table 1).

3 EXPERIMENTAL ARRANGEMENTS

3.1 INSULATOR RODS

Figure 2 shows the three types of cylindrical insulators investigated. These test objects represent typical geometries used in the medium voltage range. All objects were moulded in epoxy (Bakelite® EPR 845+EPH 845 + EPC 845), and vacuum casting technology was used to avoid voids formation within the epoxy and reduce risk for insulator puncture during testing. The relative permittivity is equal 4.0.

At the top and bottom ends of each configuration field diffusers were mounted to avoid unintended discharges at the connection with the impulse generator. Difusers are cylindrical aluminum disks that are 100 mm in diameter, 40 mm thick and have a 10 mm rounding radius. We used them in all experiments and simulations.

The main parameter varied in all configurations is the clearance *d* between the outer electrodes, which can be continously changed by gliding the cylindrical metalic rings (electrode rings) along the dielectric surface of the rods. The maximum clearances are limited by the manufacturing process of the rods and are as follows: for the configuration without embedded electrodes (Figure 2a) d_{max}=220 mm, for embedded electrodes without air gap (Figure 2b) d_{max} = 300 mm and for rods with an air gap (Figure 2c) d_{max} = 500 mm.

The selection of the rod parameters was based on preliminary Laplacian field computations that allow identification of the range of inception and withstand voltages. An example of such computations is shown in Figure 3. In all configurations there is one critical spot located on the HV electrode ring where the inception voltage calculated according to equation (1) varies with the ring distance (clearance) from 30 to 180 kV. Another inception occurs on dielectric surfaces for configurations with embedded electrodes (electrode-less inception). The corresponding inception voltages are almost independent from

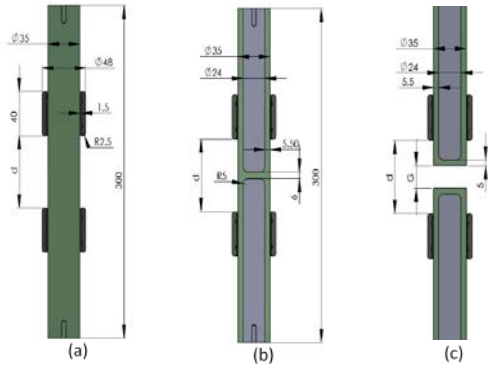

Figure 2. Three different cylindrical test configurations used in this work. a). Support insulator. b). Support insulator with two embedded electrodes. c) Two insulators with embedded electrodes with a defined air gap; the width of the gap is G = 5 mm and 20 mm

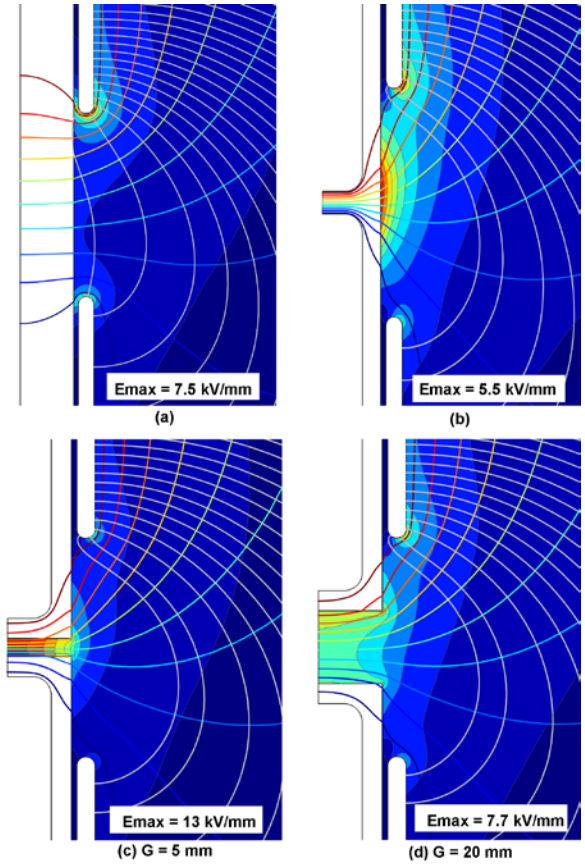

Figure 3. Calculated Laplacian field for the test configurations from Figure 2. The applied voltage is 100 kV and distance between electrode rings is 60 mm. The colour plot represents the field in air whereas the lines denote equipotential and field lines.

the ring distance and are evaluated as follows: 61.2 kV for the configuration without air gap, 25.6 kV for the 5 mm air gap and 65.6 kV for the 20 mm air gap. Based on the stability field rule (2) applied to the maximum electrode distances and the leader transition criterion (3) for 5.5 mm insulation layer we predicted the maximum withstand voltage for all tested configurations at the level of 150 kV.

3.2 EXPERIMENTAL PROCEDURE

Test objects were stressed with a standard 1.2/50 µs lightning impulse (LI) according to the IEC 60060 standards. The impulse was generated with two-stage Marx impulse generator (200 kV), and a capacitive voltage divider was connected with the oscilloscope to measure the voltage.

The temperature, pressure and humidity were recorded during the work, and the measured values of the voltage were corrected according to normalized climate conditions as defined in IEC Standard 60060.

3.2.1 MEASUREMENT OF LI INCEPTION VOLTAGE

Current monitor measurement

The discharge current was measured with a current monitor (Pearson current monitor, Model 6585, Pearson Electronics Inc., USA) connected between the test sample and ground.

Figure 4 shows the results of the measured inception current, on the support insulator with embedded electrodes. The photo was taken with a Phantom High Speed camera. The measured oscillation of the current, at around 1.2 micro seconds, indicates that there is an inception at the voltage level of 66 kV (which is very close to the calculated 65.6 kV). The photo shows the activity of partial discharges in the centre of the insulator. The photo also shows that there were several discharges around the circumference of the insulator. Because of the electromagnetic noise it was difficult to sort out the inception from the measured current. It was concluded that this was not the best method for measuring inception.

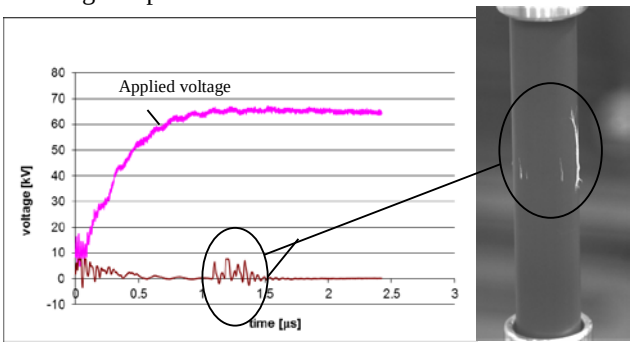

Figure 4. Measurement result with current monitor and the corresponding streamer snapshot with high speed camera

Photo multiplier tube (PMT) measurement

With a photomultiplier tube R456 from Hamamatsu, we could detect light emission from the inception. The advantage of using the PMT was that the electromagnetic noise was reduced with respect to the current measurement approach. This resulted in a better prediction of the lightning inception.

The curves in Figure 5 show measured voltage from two different shots on two support insulators with embedded electrodes. The red curve shows the measured voltage of a shot lower than the inception voltage. For an applied voltage of 82 kV (green curve), the voltage from the photomultiplier immediately increases to about 430 mV. After about 380 µs there was another peak of the measured voltage. This illustrates that restrikes occurred during the impulse.

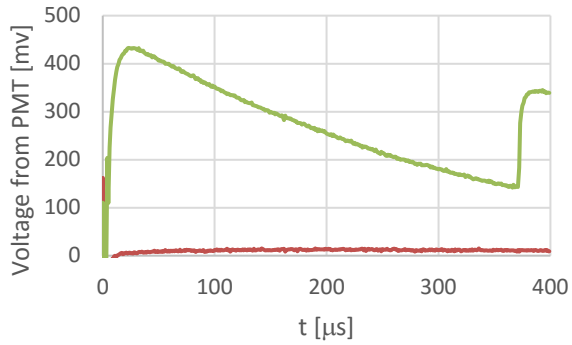

(a)

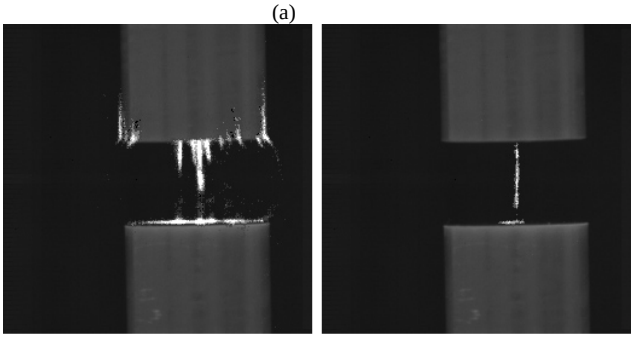

(b) (c)

Figure 5. Voltage measured with the photomultiplier (a) and high speed camera streamer pictures (b) and (c) recorded during impulse tests on the setup with embedded electrodes with gap. The gap was G = 20 mm between the insulators and the distance between the rings was d = 400 mm. The applied voltage was 82 kV. The PMT voltage steps (green curve) shown in picture (a) correspond to snapshots (b) and (c) recorded after the first few microseconds and after 380 µs, respectively.

3.2.2 MEASUREMENT OF BREAKDOWN AND WITHSTAND VOLTAGE

The LI breakdown was measured with the up- and down method. We cleaned the epoxy surface with ethanol before every shot to remove the attached surface charges and contaminations due to streamer activity. The time between every shot was 2 minutes. The number of shots per geometrical configuration was in between 20 and 30. We used the method of Maximum Likelihood [12] to estimate a normal distribution and its characteristics like 50% and the 2% quantiles that correspond to the breakdown and withstand voltages respectively. For both values, we calculated the 95% confidence intervals. Figure 6 shows the estimated breakdown and withstand voltages together with their confidence intervals (vertical lines around each experimental point). The confidence intervals specify that the estimated $U_{50\%}$ or $U_{2\%}$ values will not exceed the lower or upper limit with probability of 0.95. For example, the value $U_{2\%}$ for d = 100 mm in Figure 6a is equal to 117.7 kV, but the lower confidence interval is 21 kV less.

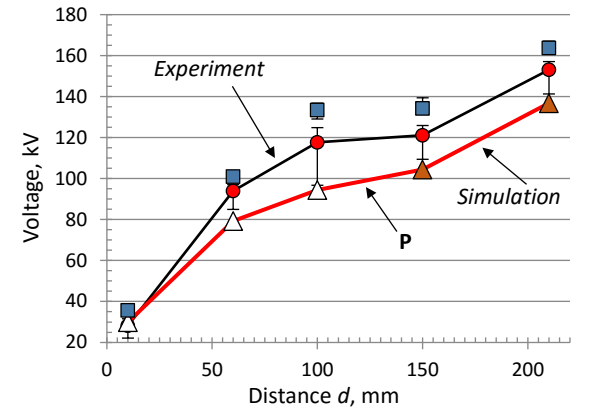

(a)

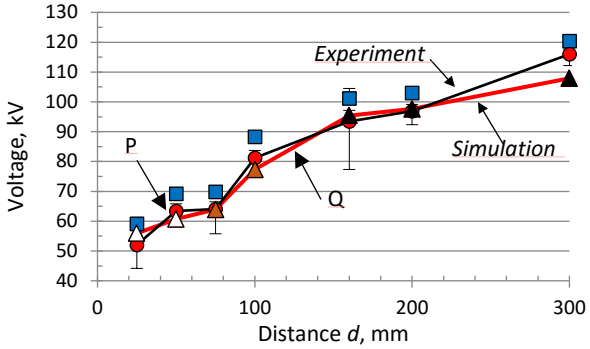

(b)

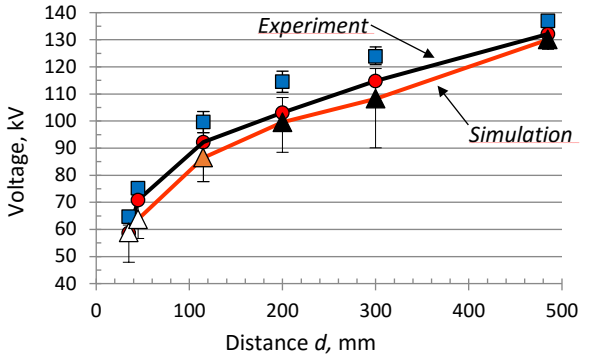

(c)

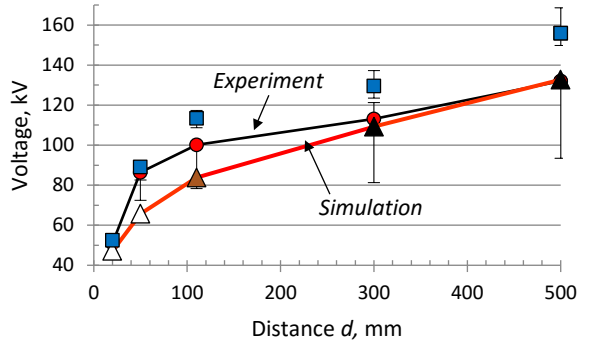

(d)

Figure 6. Results from experiments and simulations on insulator rods: (a) without embedded electrodes, (b) with embedded electrodes, no gap, (c) and (d) with embedded electrodes for air gaps 5 and 20 mm respectively. Legend: Experimentally obtained voltage: ■ 50% Breakdown ● 2% Withstand Simulation withstand voltage for: △ Inception ▲ Stability field ▲ Leader

That means: after repeating the same test series 20 times there will be one of the series for which the estimation of $U_{w2\%}$ will be lower than 96.7 kV. A large range of confidence intervals indicates unstable behavior of the propagating discharge that makes a correct prediction difficult.

4 Simulation Models for Discharge Evaluation with Surface Charging

We recognized that surface charging is an important factor that influences our experimental results. We describe in this section the concept of saturation charge and apply it to evaluation of restrikes, changed inception conditions as well as leader transition.

4.1 Saturation Charge Formulation

The basic equation applies the Gauss law to a surface region or a point on the boundary between air and insulator as follows:

$$\varepsilon_{Ins} E_{nIns} = \varepsilon_{Air} E_{nAir} + \sigma_s \quad (4)$$

where ε_{Ins} and ε_{Air} are permittivities, E_{nIns} and E_{nAir} are normal components of field strength in insulator and air respectively; σ_s is the surface charge density accumulated in air on the insulator. The equation (4) is sufficient to solve the electrostatic field problem when the value of σ_s is known (like in the case the basic Laplace field solution where $\sigma_s = 0$). In general, the value of the accumulated surface charge depends on discharge behavior and surface properties (surface conductivity), which require complex models for detailed evaluation.

This complexity can be avoided when considering only an extremal case of surface charging, which is saturation. In the saturation case, the amount of the surface charge is so large that the normal component of the field strength E_{nAir} is zero, which disables further charge accumulation:

$$E_{nAir} = 0 \quad (5)$$

After applying equation (5) to (4) and substituting σ_s by an unknown saturation charge density σ_{sat}, the continuity equation is expressed as follows:

$$\varepsilon_{ins} E_{nIns} = \sigma_{sat} \quad (6)$$

Splitting the continuity equation (4) into two separate parts equations (5) and (6) increases the number of equations in the electrostatic formulation but this is required in order to solve for unknown σ_{sat}. The implementation of equations (5) and (6) is straightforward for the indirect integral formulations of electrostatic problems [13,14]. For the purpose of the analysis presented in this paper we have implemented equations (5) and (6) as a new boundary condition in the axisymmetric formulation of the region-oriented charge simulation method [13].

The locations of the saturation charge boundary condition depend on the availability of charge supplied by the propagating streamers. A precise approach may require an iterative procedure that estimates these locations in each step until no change occurs. For the basic geometries investigated in this paper, it is sufficient to predefine the location of saturation charges, as explained in the next subsections.

4.2 EVALUATION OF RESTRIKES

The experimental results shown in Figure 5c confirm the evidence of surface charge. This result indicates that the layer of surface charge accumulated during the first few microseconds of the lightning impulse on the horizontal surfaces of both rods is large enough to cause a re-inception of the streamer discharge after a few hundred microseconds (when the HV electrode is almost at zero potential).

When simulating this phenomenon, one needs to consider two additional stages (in addition to the first "Laplacian field stage" shown in Figure 3d). The second stage describes the field with saturation charge while the applied voltage is still at the maximum level and the third stage uses the same saturation charge when the HV electrodes are at zero potential.

For the second stage, the locations of application of the saturation charge boundary condition must be specified, i.e. on which surfaces the charge carried by streamers can be deposed. An electrodeless inception and the double-headed streamers initiated in the gap between rods leave positive charges on the lower rod while the negative charges accumulate on the upper one. The horizontal surfaces of both rods are the most exposed surfaces for charge accumulation; however, the propagating discharge may also affect the vertical cylindrical surfaces. Therefore, the saturation charge boundary condition applies to all dielectric surfaces exposed to air up to the electrode rings. It is not required to specify the polarity of the saturation charge: it will be obtained as a solution of equations (5) and (6).

For the third stage, we use the saturation charge calculated in the second stage and apply it as the known charge σ_s in equation (4). In this case, all electrode potentials are set to zero, so that the only excitation comes from the surface charge. Figure 7 shows the results for both stages involving surface charge. For the second stage, the saturation charge has a strong "damping" effect in the region between rods, which is now almost "field-less". In the third stage, the field strength distribution in air and consequently the resulting inception voltage of 65.6 kV are in fact identical to the initial stage without surface charges (shown qualitatively in Figure 3d). Only the orientation of the field vectors is reversed due to inverted potential values.

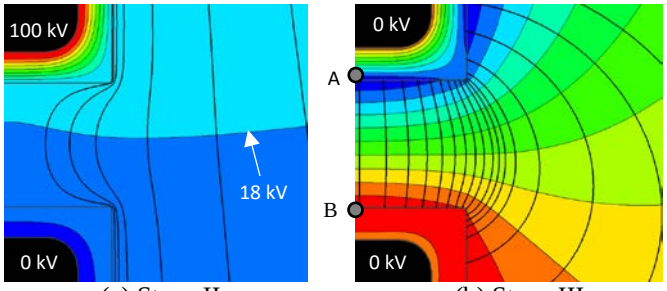

(a) Stage II (b) Stage III

Figure 7. Potential distribution and field lines in the gap between insulator rods (G = 20 mm, d = 400 mm) calculated with saturation charge boundary condition for two stages of the applied voltage (a) 100 kV and (b) 0 kV. The values of surface charge density calculated in points A and B are: -580 pC/mm^2 and 130 pC/mm^2 respectively. The corresponding values of potential are: -74.5 kV and 11.5 kV whereas the electric field strength in both inception points are 5.0 kV/mm and 4.4 kV/mm.

It is not surprising since the field in the gap is determined by the perfectly saturated surface charge, fully reflecting the conditions of the initial background field (no decrease of charge due to insufficient charging or surface conductivity has been assumed). Restrikes occurring in the experiments for the applied voltage of ~82 kV and above confirm this simulation result. The analysis of charging stage III can be also performed for the changed polarity of the applied voltage. In case of - 100 kV applied to the upper electrode the field strength in the gap calculated together with remaining surface charge will be doubled and the inception voltage reduced significantly. This approach provides an opportunity to evaluate reduced inception voltage for arrangements with surface charging and changing polarity (like AC or LI- after LI+).

4.3 INCEPTION VOLTAGE IN SATURATED STAGE

The accumulated saturation charge significantly influences the distribution of the field strength and consequently changes the inception conditions during the impulse test. The surface charge may have a mitigating effect in some critical spots but can create discharge inception in new locations that would not have been critical without the presence of surface charge. In the following 2 subsections, we show the influence of the accumulated saturation charge on streamer inception and propagation conditions for the insulating rods without and with embedded electrodes (Figure 2a and b)

4.3.1 INCEPTION AT ELECTRODE

For the insulating rod without the embedded electrodes, the initial inception occurs at the HV electrode as shown in Figure 8. Due to inception at the inner side of the HV shielding ring the positive streamers will propagate on to the surface of the insulator, deposing positive charge. In this case, the negative charge carriers are not available (there is no inception at grounded electrode).

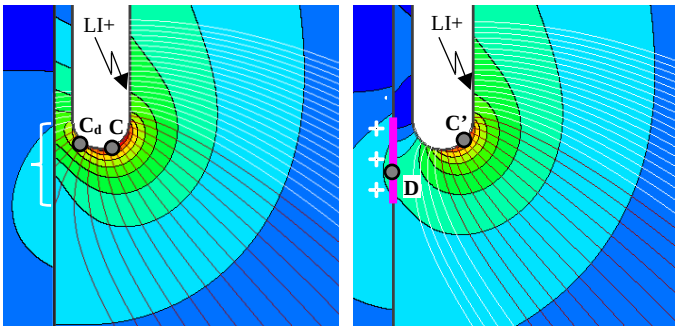

(a) Stage I (b) Stage II

Figure 8. Field strength distribution and field lines calculated around the tip of the upper ring electrode for the arrangement without embedded electrodes (d = 100 mm, U_{app} = 100 kV) (a) without surface charge, (b) with the positive saturation charge accumulated around point D on the insulator surface (thick magenta line). All field lines start at surface points with the field strength larger that the critical value 2.6 kV/mm. The inception occurs for dark lines whereas for white ones there is no inception (according to criterion (1)). The maximum surface charge density in point D is 59 pC/mm^2. The maximum field strength calculated in both stages for points C and C' is 6.6 kV/mm and 6.2 kV/mm respectively. The corresponding inception voltages at these points are 78.2 kV and 82.7 kV. The point C$_d$ marks the inception location that leads to a streamer hitting the insulator surface. The field strength in point C$_d$ is 5.4 kV/mm and the inception voltage 94.4 kV.

Therefore when specifying the location of the saturation charge boundary condition, one has to take care that only positive charge density will be obtained from solving equations (5) and (6). This can be achieved by setting the surface charge boundary condition only in locations where the inception streamlines hit the insulator surface (white brace in Figure 8a). Alternatively, we can define this boundary condition only for locations where the normal component of the background field calculated in Stage I is pointing out of the insulator. Both approaches lead to approximately the same result, which is shown in Figure 8b.

4.3.2 ELECTRODELESS INCEPTION

Figure 9 illustrates the charge accumulation on the support insulator with embedded electrodes. A double-headed streamer starts from the electrodeless inception spot D, and deposes negative and positive surface charge on the dielectric surface when propagating towards electrodes. The deposed charge mitigates the high field strength at the initial point D (Figure 9b), however the accumulation of the negative saturation charge contributes to increased field strength at the point C' and consequently a new positive streamer discharge can be initiated at the HV electrode ring.

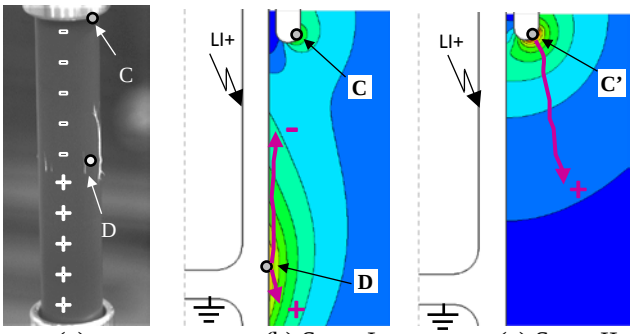

Figure 9. Influence of saturation charge on field strength and inception voltage: (a) charge accumulation due to propagation of a double-headed streamer; (b) field strength computed without surface charge; (c) field strength computed with the saturation charge on the insulator surface. The field strength values at points C, D and C' are 4.3, 5.6 and 6.9 kV/mm, respectively. The corresponding values of inception voltage are: 116.3, 61.2 and 74.1 kV. The streamers propagating from D and C' may lead to a breakdown only if the stability field criterion (2) is satisfied, i.e. for the applied voltage larger than 77.4 kV. All values are valid for electrode clearance in air d = 100 mm and U_{app} = 100 kV.

4.4 EVALUATION OF LEADER TRANSITION

The crucial parameter for evaluation of leader transition voltage is the surface capacitance (3). Based on saturation charge we can calculate it for every surface point as follows:

$$c' = \left|\frac{\sigma_{sat}}{\Delta U_{ins}}\right| \tag{7}$$

where σ_{sat} is the saturation charge density calculated according to equations (5) and (6) , ΔU_{ins} is the voltage drop between the charged point on the insulator surface and the closest electrode.

As an example, Figure 10 shows the distribution of σ_{sat}, ΔU_{ins} and c' for insulating rod with two embedded electrodes (Figure 2b) and the electrode ring distance d = 100 mm. In spite of the electrical asymmetry, which is visible in σ_{sat} and ΔU_{ins} distributions, the surface capacitance c' is symmetric and closely matches the analytically calculated value for the cylindrical insulation layer. This result demonstrates that the saturation charge concept enables the numerical calculation of surface capacitance along the discharge path for arbitrary geometries.

For proper estimation of leader transition characteristics one should take into account not only varying values of c' but also the voltage drop ΔU_{ins} across the insulation layer, which varies along the path of the propagating discharge. In other words, one desires to find the minimum voltage applied to the active electrode that will result in leader transition at the most critical point x along the discharge path. We propose to calculate this voltage as follows:

$$U'_{0L} = \min_x\left(\left|\frac{U_{app}}{\Delta U_{ins}}\right| U_{0L}\right) \tag{8}$$

where U_{0L} is evaluated according to equation (3) and U_{app} is the applied voltage that has been used for the numerical computation of ΔU_{ins}. Figure 10 shows a computation example of U_{0L}'.

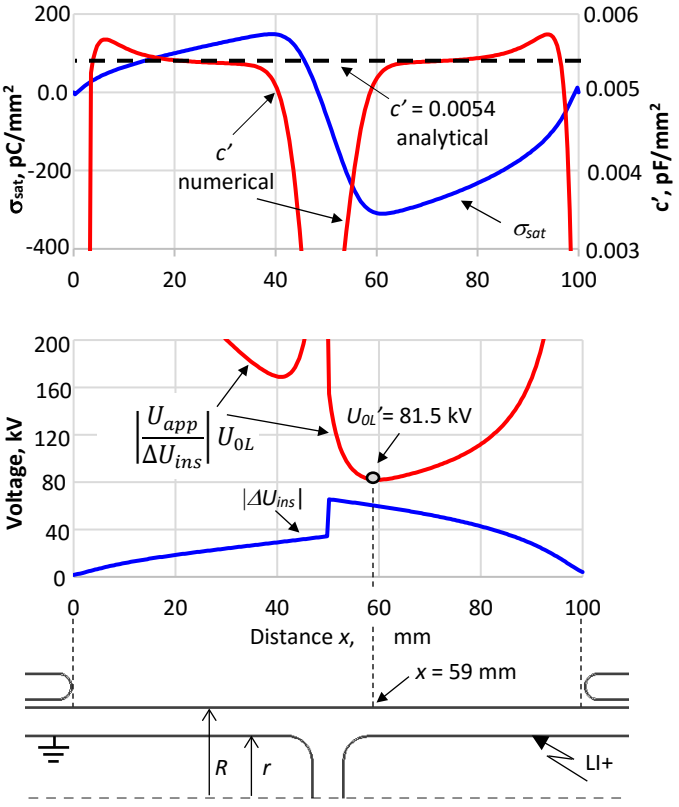

Figure 10. Evaluation of leader inception voltage based on computation of saturation charge for insulator rod with d = 100 mm and U_{app}= 100 kV. The analytical surface capacitance is calculated as $c'=\varepsilon_{Ins}/(R\ln(R/r))$. Comment: The obtained leader inception voltage of 81.5 kV is larger than the withstand value 77.4 kV resulting from streamer analysis shown for the same arrangement in Figure 9. Consequently, the leader transition will not occur for d = 100 mm, but will be the dominating breakdown phenomenon for larger electrode distances.

The corrected leader transition voltage U_{0L}' can be conservatively interpreted as the withstand voltage since the leader behavior is difficult to predict and may result in

punctures. However, the real withstand voltage is larger than U_{0L}' due the fact that the leader itself will require an additional voltage to reach the electrodes. In order to enable a comparison with experimental values we estimate the withstand voltage U_{wL} as follows:

$$U_{wL} = U'_{0L} + d \cdot E_L \quad (9)$$

where E_L is the internal field strength required for leader propagation over the distance d between electrodes. We assume here E_L= 0.15 kV/mm. However, we strongly recommend replacing this type of evaluation by a physical leader model based on numerically computed surface capacitance.

5 Discussion of Results

We applied the discharge model described in section 2 and the saturation charge concept from section 4 to evaluate the withstand voltage of the experimental arrangements. Table 2 summarizes the details of this evaluation for the insulating rod with embedded electrodes (Figure 2b). This Table includes values of critical voltages computed for all discharge and charging stages as well as the experimental withstand voltage. The computed voltages that are relevant for the final prediction are marked in red color whereas the yellow color denotes voltages that initiate the different discharge stages (like inception of streamer or transition to leader), however, are not sufficient for the breakdown. The comparison of measured and computed values in Figure 6b shows a good agreement between the two sets of data.

Table 2. Voltages calculated and measured for insulator rod with embedded electrodes. Explanations: U_{iC} and U_{iD} are streamer inception voltages calculated without surface charge (Stage I) whereas U_{iC}' is calculated with the saturation charge (Stage II). Figure 9 shows the locations of the points C, D, and C'. U_{wS} is the withstand voltage based on streamer stability rule (2), U_{0L}' is the corrected leader transition voltage equation (8) and U_{wL} is the leader withstand voltage equation (9). $U_{w2\%}$ is the 2% withstand voltage measured experimentally. All voltages are in kV.

d mm	U_{iC}	U_{iD}	U_{iC}'	U_{wS}	U'_{oL}	U_{wL}	$U_{w2\%}$ test
25 [1]	55.9	57.5	51.5	36.9	163.6	167.3	52.1
50 [2]	84.3	60.7	64.9	50.4	107.3	114.8	63.4
75 [3]	103.1	61.1	70.8	63.9	90	101.2	64.0
100 [4]	116.3	61.2	74.1	77.4	81.5	96.5	81.2
160 [5]	139.7	61.3	79.0	109.8	71.4	95.4	93.4
200 [5]	155.0	61.3	82.4	131.4	67.6	97.6	96.9
300 [5]	n.a. [6]	61.3	n.a. [6]	185.4	62.9	107.9	116.0

[1] Inception at the HV shielding ring leads immediately to breakdown.
[2] Streamer propagating from electrode-less inception may bridge the gap between electrode rings; Stable streamer propagation is ensured since $U_{wS} < U_{iD}$
[3] Inception mechanism is the same as in 2), but the breakdown can only occur if stability rule is satisfied and therefore U_{wS} determines the withstand level.
[4] Same as for 3) but another streamer started from the ring electrode supports the breakdown development (Figure 9).
[5] The leader transition occurs before the streamer can bridge the gap between electrodes ($U_{wS} > U_{0L}$'). Furthermore, in all 3 cases, the roughly estimated U_{wL} is lower than U_{wS}, which confirms that the leader mechanism dominates the breakdown process.
[6] We removed the electrode rings in order to utilize the full length of the insulator rod (only field diffusers were mounted to the rod ends). Therefore the inception points C and C' on the electrode ring are removed.

It is possible to distinguish between the 3 stages of the discharge indicated in the basic concept presented in **Figure 1** and to identify the location of points P and Q marking the border between the different phenomena responsible for the withstand voltage.

The results for the support insulator without embedded electrodes (Figure 2a) show the largest deviations between experiment and simulation for electrode distance range 60-100 mm, see Figure 6a. According to the results presented in subsection 4.3.1 both the lowest inception voltage as well as the lowest withstand voltage resulting from the stability field equation (2) are evaluated at the level of ~80 kV. In comparison, the experimentally obtained 2% withstand voltage of ~118 kV is significantly higher. On the other hand, the $U_{w2\%}$ has surprisingly wide confidence intervals, which indicates a likelihood that multiple discharge mechanisms or processes are responsible for the final breakdown. In the particular case of d = 100 mm, we have identified two possible paths of discharge propagation: directly along insulator surface and the lateral path, in the bulk air. The latest experimental investigations [15] confirm the evidence of surface and bulk discharges, which have been observed during an impulse applied in a similar configuration: HV-rod, insulator parallel to field direction and the ground. Interestingly, streamers creeping along insulators are significantly faster than streamers in bulk gas. However, engineering models that allow quantitative assessment of breakdown/withstand voltage for streamers propagating in atmospheric air are not yet available.

The streamers along insulators have a shorter path (~100 mm) that according to equation (2) can lead to a breakdown even for the lowest inception voltage calculated for this configuration. However, the inception level for streamers propagating onto the insulator surface is in the range of ~94 kV and larger (see results for the point C_d in Figure 8a). Therefore, for the surface discharges along the insulator surface we can estimate the withstand voltage as 94 kV, which is very close to the experimentally obtained lower limit of the confidence interval.

The lateral discharge in bulk air seems to require more voltage (and energy) in order to reach the grounded electrode. The possible charge accumulation due to streamer activity and deposing charge at the insulator surface provides an additional force "pushing out" the discharge from the insulator making the path longer. The length of the field lines calculated from point C', Figure 8, are in the range of 170 mm until they reach the grounded electrode. Using this length in stability criterion (2) would allow a perfect agreement between the predicted and measured withstand voltages. However, in general, a field line based approach is not correct since field lines do not follow the discharge path. Therefore, for the arrangement in Figure 2a we limit our prediction to the discharge creeping along insulator, for which the stability criterion is fulfilled and the enhanced inception voltage determines the withstand voltage prediction (94 kV for d = 100 mm and 79 kV for 60 mm). This approximation still deviates from the experimental $U_{w2\%}$ values, but in a way that ensures a safety margin needed in engineering. Such deviations indicate that the stability field concept based on clearance in air may require a major revision, in particular for lateral inceptions. The research in this area is still ongoing.

In case of embedded electrodes with air gap, the largest deviation between experiment and simulation occurs for the air gap of 20 mm and electrode distances in the range of 50-100 mm, see Figure 6d. We explain the high experimental withstand voltages by the fact that the charge accumulation is limited to the air gap between rods whereas the vertical rod surfaces are not affected. Due to lack of accumulated negative charge (shown in Figure 9a), the inception at the ring will occur at a higher voltage level and it will be lateral like in the case without embedded electrodes. This indicates that in addition to lateral inception the placement of the saturation charge boundary condition needs further investigations.

6 Conclusion

A combination of the traditional discharge model and the numerical field computation based on the concept of saturation charge enabled an acceptable prediction of the withstand voltage for insulating rods investigated in this work. The new formulation allows re-calculation of the inception conditions due to charge accumulation, while also providing an opportunity of numerical evaluation of surface capacitance and related conditions of discharge (leader) propagation. For further improvements, we see a need for a better estimation of charge accumulation during the discharge, in particular a precise placement of the saturation charge boundary condition. We also recommend revising the discharge propagation concepts including stability field and leader transition.

The new methodology is simple enough to be applicable in engineering environments. Therefore, we expect further progress from future applications of this approach. The latest work on charging of dielectric barriers [16] shows encouraging results.

Acknowledgment

We dedicate this paper to memory of Prof. Helmut Böhme. He significantly contributed to the development of the presented prediction approach cooperating with the authors over 20 years.

We thank our colleagues from ABB Corporate Research Switzerland and ETH Zurich for the fruitful discussions and support.

References

[1] E. Philipow, Taschenbuch Electrotechnik, Verlag Technik Berlin, 1982.
[2] H. Böhme, Mittelspannungstechnik, Verlag Technik Berlin, 2005.
[3] A. Küchler, Hochspannungstechnik. Springer-Verlag Berlin-Heidelberg, 2009.
[4] A. Dubinova, Modeling of streamer discharges near dielectrics, PhD. TU Eindhoven, 2016 (ISBN : 978-90-386-4128-7).
[5] A. Pedersen, T. Christen, A. Blaszczyk, H. Boehme, "Streamer inception and propagation models for designing air insulated power devices", IEEE Conf. Electr. Insul. Dielectr. Phenomena (CEIDP), pp. 604-607, 2009.
[6] A. Blaszczyk, H. Boehme, A. Pedersen, M. Piemontesi, "Simulation based spark-over prediction in the medium voltage range", International Symposium on High Voltage Engineering (ISH), pp. 205-206, 2001.
[7] K. Petcharaks: "Applicability of the Streamer Breakdown Criterion to Inhomogenous Gas Gaps", Ph. D. Thesis No. 11192, ETH Zurich, 1995.
[8] N. Allen, P.N. Mikropoulos, "Streamer propagation along insulating surfaces", IEEE Trans. on Dielect. and Electr. Insul. Vol. 6. No.3, pp. 357-362, 1999.
[9] L. Pritchard, N. Allen, "Streamer propagation along profiled insulator surfaces", IEEE Trans. on Dielect. and Electr. Insul. Vol. 9 No. 2, pp. 371-380, 2002.
[10] L. Lazaridis L., P.N. Mikropoulos, "Flashover along cylindrical insulating surfaces in a nonuniform field under positive switching impulse voltages", IEEE Trans. on Dielect. and Electr. Insul. Vol. 15, No 3, pp. 694-706, 2008.
[11] F. Mauseth, J.S. Jorstad, A. Pedersen, "Streamer inception and propagation for air insulated rod-plane gaps with barriers", Conf. Electr. Insul. Dielectr. Phenomena (CEIDP), pp. 729-732, 2012.
[12] J. Speck: Statistische Auswertung experimenteller Daten zur Alterung Elektrotechnischer Betriebsmittel. Scientific Conference of Sect. Electrotechnics, TU Dresden, paper H2-08, 1987.
[13] A. Blaszczyk and H. Steinbigler. Region-oriented charge simulation. IEEE Trans. on Magnetics, vol 30, no. 5, pp. 2924–2927, 1994.
[14] N. De Kock, M. Mendik, Z. Andjelic and A. Blaszczyk. Application of 3D boundary element method in the design of EHV GIS components. IEEE Magazine on Electrical Insulation., Vol.14, No. 3, pp. 17–22, 1998.
[15] D. Trienekens, Experiments on streamer interaction with dielectric surfaces. PhD. Thesis, TU Eindhoven, 2016 (ISBN: 078-90-386-4082-2).
[16] A. Blaszczyk, J. Ekeberg, S. Pancheshnyi, M. Saxegaard, Virtual High Voltage Lab, In "Scientific Computing in Electrical Engineering - SCEE 2016", ed. by U. Langer, W. Amrhein, W. Zulehner, Mathematics in Industry, Springer, Heidelberg, 2017 (to appear).

Atle Pedersen received the M.Sc. degree and the PhD degree in electrical power engineering from the Norwegian University of Science and Technology (NTNU), Trondheim, Norway in 1994 and 2008 respectively. He has worked at ABB Distribusjon in Skien Norway from 1994 – 2001. He has been in SINTEF Energy Research since 2006. His field of interest include high-voltage switchgear, power cables, and testing of high voltage apparatus. His research work also includes dielectric, electromagnetic and electro thermal simulations of power devices.

Pedersen has also had a post doc position at the high voltage laboratory at the Swiss Federal Institute of Technology (ETH Zürich). All experimental work presented in this paper was performed during the post doc project.

Andreas Blaszczyk received the M.Sc. and PhD degrees in 1979 and 1984 from the Electrical Engineering Faculty of the Silesian Technical University Gliwice, Poland where he continued to work on simulation of electric power systems until 1987. From 1988 he was a researcher at the Technical University Munich in the area of simulation of electric fields in high voltage engineering. In 1990 he joined ABB Corporate Research in Heidelberg/Germany and in 2003 he switched within the same organization to Baden/Switzerland. His research work at ABB includes dielectric, thermal and electromechanical simulation of power devices as well as the high performance computing.